

# Modeling silica aerogel optical performance by determining its radiative properties

Cite as: AIP Advances 6, 025123 (2016); <https://doi.org/10.1063/1.4943215>

Submitted: 22 November 2015 • Accepted: 22 February 2016 • Published Online: 29 February 2016

 Lin Zhao,  Sungwoo Yang, Bikram Bhatia, et al.



View Online



Export Citation



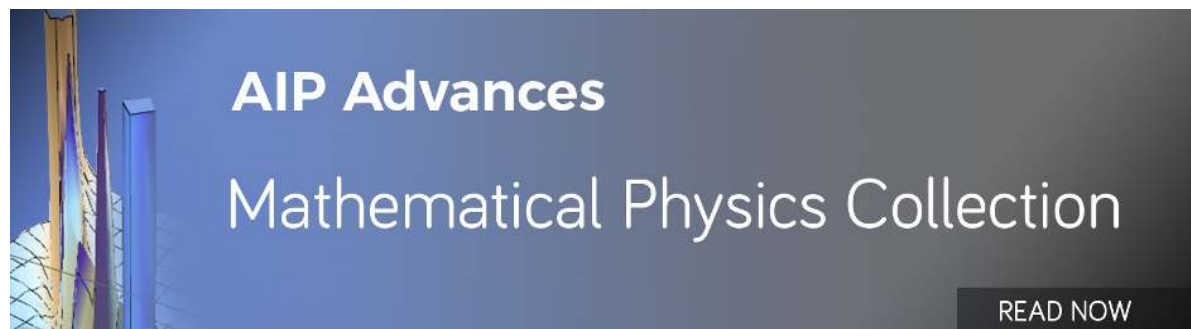
CrossMark

## ARTICLES YOU MAY BE INTERESTED IN

[High temperature stability of transparent silica aerogels for solar thermal applications](#)  
APL Materials **7**, 081104 (2019); <https://doi.org/10.1063/1.5109433>

[Erratum: "Modeling silica aerogel optical performance by determining its radiative properties" \[AIP Advances 6, 025123 \(2016\)\]](#)  
AIP Advances **6**, 099901 (2016); <https://doi.org/10.1063/1.4962765>

[Plasmonic absorption-induced haze suppression in random scattering media](#)  
Applied Physics Letters **114**, 251102 (2019); <https://doi.org/10.1063/1.5100512>



AIP Advances  
Mathematical Physics Collection

READ NOW



## Modeling silica aerogel optical performance by determining its radiative properties

Lin Zhao, Sungwoo Yang, Bikram Bhatia, Elise Strobach,  
and Evelyn N. Wang<sup>a</sup>

*Department of Mechanical Engineering, Massachusetts Institute of Technology, Cambridge, Massachusetts 02139, USA*

(Received 22 November 2015; accepted 22 February 2016; published online 29 February 2016)

Silica aerogel has been known as a promising candidate for high performance transparent insulation material (TIM). Optical transparency is a crucial metric for silica aerogels in many solar related applications. Both scattering and absorption can reduce the amount of light transmitted through an aerogel slab. Due to multiple scattering, the transmittance deviates from the Beer-Lambert law (exponential attenuation). To better understand its optical performance, we decoupled and quantified the extinction contributions of absorption and scattering separately by identifying two sets of radiative properties. The radiative properties are deduced from the measured total transmittance and reflectance spectra (from 250 nm to 2500 nm) of synthesized aerogel samples by solving the inverse problem of the 1-D Radiative Transfer Equation (RTE). The obtained radiative properties are found to be independent of the sample geometry and can be considered intrinsic material properties, which originate from the aerogel's microstructure. This finding allows for these properties to be directly compared between different samples. We also demonstrate that by using the obtained radiative properties, we can model the photon transport in aerogels of arbitrary shapes, where an analytical solution is difficult to obtain. © 2016 Author(s). All article content, except where otherwise noted, is licensed under a Creative Commons Attribution (CC BY) license (<http://creativecommons.org/licenses/by/4.0/>). [<http://dx.doi.org/10.1063/1.4943215>]

### I. INTRODUCTION

Silica aerogels have attracted research and industrial interest due to its unique properties: low density, large specific surface area, low refractive index, high transparency and low thermal conductivity. The microstructure of the aerogel, comprised of cross-linked particles (primary particles) which form an open cell and highly porous network, gives rise to its unusual combination of properties.<sup>1-4</sup> In particular, the optical transparency of silica aerogel in the solar spectrum is crucial for many solar related applications<sup>5-8</sup> and has been studied extensively.<sup>9-18</sup> J. Fricke *et al.* showed that the optical transparency of silica aerogels is tied closely to its microstructure which acts as Rayleigh scattering centers.<sup>12,19,20</sup> A. J. Hunt performed detailed studies on scattering in silica aerogels and suggested that the transmittance and scattering can be correlated by<sup>11</sup>

$$\tau = A \times \exp\left(-\frac{B}{\lambda^4}t\right) \quad (1)$$

where  $\tau$  is the transmittance.  $A$  is the wavelength independent coefficient accounting for surface defects,  $B$  describes the extinction contribution from the Rayleigh scattering, and  $t$  is the thickness of the sample. Eq. (1) and its coefficients, sometimes referred to as the “Hunt parameters”, have been widely used to compare the clarity of silica aerogels of various thicknesses, origins, and surface conditions and to separate their intrinsic and extrinsic qualities.<sup>5,12,13</sup>

<sup>a</sup>enwang@mit.edu

Although convenient to use, Eq. (1) has two major limitations. Firstly, the wavelength dependent extinction contribution includes only scattering, which limits its use to the spectrum where absorption is negligible. Secondly and more importantly, in the spectrum range where scattering is dominant, the exponential form of Eq. (1), which is based on the Beer-Lambert (B-L) law, can be inaccurate. The B-L law focuses on a single propagation direction. But in the case of silica aerogel, a highly scattering medium, all propagation directions are coupled because of the multiple scattering effect.<sup>21</sup> As a result, the B-L law may not be adequate to describe this multi-directional radiation transfer problem especially in applications where hemispherical (direct + diffuse) instead of directional flux is of interest.

To fully capture the multi-directional nature of this problem, we introduced a model based on the 1-D Radiative Transfer Equation (RTE). In previous studies, the RTE has been used to investigate the radiative properties of silica aerogels in the infrared spectrum,<sup>22,23</sup> which have significant effects on the thermal insulating properties. The RTE has also been applied to silica nanoporous matrices, a material made by pressure packing off-the-shelf silica nanoparticles, to study its radiative properties in the solar and infrared spectrum.<sup>24</sup> In this study, we applied our RTE model to in-house synthesized silica aerogels and focused on the optical properties in the solar spectrum. Two sets of wavelength dependent radiative properties, the absorption and scattering coefficient, were deduced from the model based on experimentally measured transmittance and reflectance spectra. Compared to Eq. (1), the RTE model captures both the scattering and absorption contribution and can predict the optical performance of aerogel with improved accuracy. The deduced radiative properties, which were found to be independent of sample thickness, quantifies the absorption and scattering separately. These properties can be considered the intrinsic optical properties to compare different samples as well as to study photon transport in silica aerogel samples with complex geometries, where it is difficult to find an analytical solution.

## II. EXPERIMENT

Silica aerogels are commonly produced by a sol-gel process, followed by critical point drying to extract all of the solvent. The synthesis procedure in this study is described in the supplemental section I,<sup>25</sup> which is based on previous work.<sup>26</sup>

We prepared eight aerogel samples ( $20 \times 20 \text{ mm}^2$ ) with thicknesses between 1 mm and 11 mm. Thinner samples were obtained by carefully removing excess materials from an 11 mm sample using a grit 1000 sand paper.<sup>27</sup> The aerogel samples were then optically characterized by a UV-Vis-NIR spectrophotometer (Cary 5000, Agilent). Hemispherical transmittance and hemispherical reflectance were measured from 250 nm to 2500 nm with a polytetrafluoroethylene (PTFE) coated integrating sphere (Internal DRA-2500, Agilent). Reflectors made of polished aluminum (Valumax Mirror, Newport, reflectivity > 90% over 250 nm to 600 nm, matching the scattering dominant region of the sample) were mounted around the four side surfaces of the sample to reflect the light exiting from the side surfaces back into the sample. By doing so, we effectively imposed a periodic boundary condition at the side surfaces and made the sample equivalent to a semi-infinitely large medium which can be more accurately captured by the 1-D model.

Figure 1 shows the obtained spectra of three representative samples of thickness 1.1 mm, 5.5 mm and 10.5 mm. The transmittance decreases with increasing sample thickness across the whole spectrum. We observed absorption peaks around 1.4  $\mu\text{m}$ , 1.9  $\mu\text{m}$  and 2.2  $\mu\text{m}$  wavelengths. On the other hand, the reflectance does not depend on the sample thickness and remains zero for wavelengths above 1.5  $\mu\text{m}$ . For wavelengths below 1.5  $\mu\text{m}$ , the reflectance increases as the wavelength decreases and thicker samples have higher reflectance. The distinct nature of absorption and scattering can be readily seen by comparing the correlation between the transmittance and reflectance spectra. For wavelengths above 1.5  $\mu\text{m}$ , the transmittance does not correlate with the reflectance. On the contrary, for wavelength below 1.5  $\mu\text{m}$ , they show a negative correlation: when the transmittance decreases, the reflectance increases. This result is expected since scattering will simultaneously reduce transmittance and increase reflectance due to more photons being backscattered.

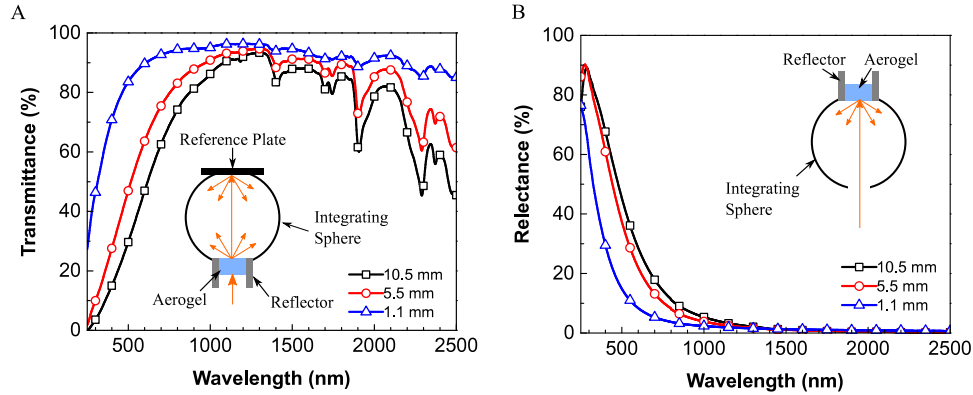


FIG. 1. Results of UV-Vis-NIR measurements: (A) hemispherical transmittance; (B) hemispherical reflectance. Transmittance and reflectance measurements were performed on eight samples of different thicknesses (1 to 11 mm). Insets show schematics of the measurements. Reflectors made of polished aluminum were mounted around the sample to minimize the side loss.

### III. MODELING

To deduce the intrinsic radiative properties of the aerogel samples, a model is needed to link the desired properties to the measured transmittance and reflectance. In this regard, the RTE is useful since it accounts for the absorption and scattering simultaneously.<sup>24,28–30</sup> In our model, we treated the aerogel as a homogeneous absorbing and scattering medium. Our main goal was to decouple the extinction contribution from absorption and scattering by identifying the absorption ( $\sigma_a$ ) and scattering ( $\sigma_s$ ) coefficient at each wavelength. The 1-D azimuthal symmetric RTE describing the radiation intensity as a function of polar angle and spatial position can be written as<sup>31</sup>

$$\mu \frac{\partial I_\lambda(\xi_\lambda, \mu)}{\partial \xi_\lambda} = -I_\lambda(\xi_\lambda, \mu) + \frac{\omega_\lambda}{2} \int_{-1}^1 I_\lambda(\xi_\lambda, \mu') d\mu' \quad (2)$$

where  $\mu = \cos(\theta)$  is the cosine of the polar angle with respect to the incident direction.  $\xi = \beta x$  is the optical depth where  $\beta_\lambda = \sigma_a + \sigma_s$  is the extinction coefficient and  $x$  is the spatial coordinate along the incident direction ( $0 < x < t$ ,  $t$  is the sample thickness).  $\omega = \sigma_s/\beta$  is the scattering albedo ( $0 < \omega < 1$ ). Wavelength dependent quantities are indicated by subscript  $\lambda$ . In Eq. (2), the thermal emission is neglected and the scattering due to the nanoscale particle is assumed to be isotropic, known as the transport approximation.<sup>21,32,33</sup> ( $\sigma_a, \sigma_s$ ) and ( $\beta, \omega$ ) are interchangeable using the following relations

$$\begin{aligned} \sigma_a &= (1 - \omega) \beta \\ \sigma_s &= \omega \beta \end{aligned} \quad (3)$$

When  $\omega = 0$  (a pure absorbing medium), Eq. (2) reduces to a first order ordinary differential equation, which can be readily integrated to get the solution as an exponential function (the B-L law). When  $\omega > 0$  (an absorbing and scattering medium), Eq. (2) becomes an integro-differential equation and needs to be solved numerically.

Since the aerogel's refractive index is very close to one,<sup>15,34</sup> the two boundary conditions at  $x = 0$  and  $x = t$  used to solve the RTE are

$$\begin{cases} I_\lambda(0, \mu) = \Phi, & \text{if } \mu_0 \leq \mu \leq 1 \\ I_\lambda(0, \mu) = 0, & \text{if } 0 < \mu < \mu_0 \\ I_\lambda(\xi(x=t), \mu) = 0 & \text{for } \mu \leq 0 \end{cases} \quad (4)$$

where  $\Phi$  is the incident flux and  $\mu_0$  is very close to 1 indicating a near collimated normal incident beam. We solved the 1-D RTE by the discrete ordinate method (DOM) with the above defined boundary conditions.<sup>31</sup> After the intensity field was obtained, the hemispherical transmittance  $\tau^h$

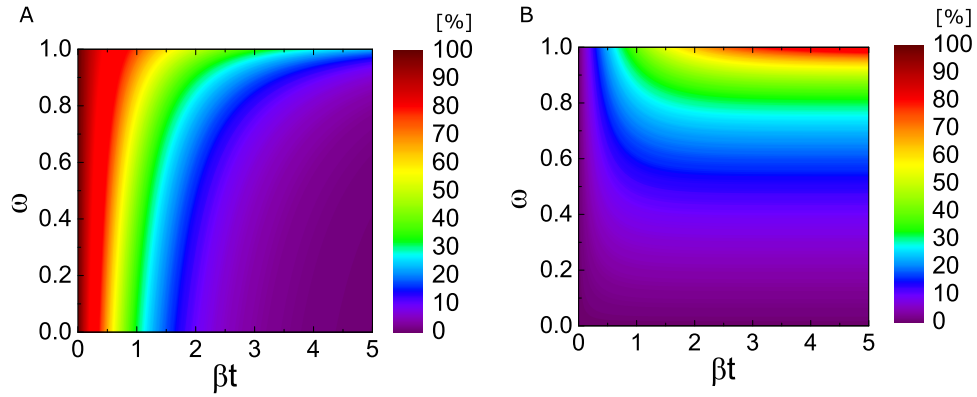


FIG. 2. Calculated hemispherical transmittance (A) and hemispherical reflectance (B) as a function of optical depth  $\beta t$  and scattering albedo  $\omega$ .

and hemispherical reflectance  $\rho^h$  can be computed as the directional sum of the transmitted or reflected intensity normalized by the incident flux

$$\tau^h = \frac{\int_0^1 I_\lambda(\xi(x=t), \mu) \mu d\mu}{\int_{\mu_0}^1 \Phi \mu d\mu}, \rho^h = \frac{-\int_{-1}^0 I_\lambda(\xi(x=0), \mu) \mu d\mu}{\int_{\mu_0}^1 \Phi \mu d\mu} \quad (5)$$

Figure 2 shows the calculated hemispherical transmittance and reflectance as a function of optical depth and scattering albedo. For scattering albedo  $\omega = 0$ , the reflectance remains zero and the transmittance reduces to the B-L law (exponential attenuation). For scattering albedo  $\omega > 0$ , the reflectance is larger than zero and the transmittance deviates from the B-L law.

The above procedure of calculating the hemispherical transmittance and reflectance based on the known optical depth and scattering albedo is often referred to as the forward problem. In reality, we are solving the inverse problem: with experimentally measured transmittance and reflectance data, we would like to evaluate the radiative properties of the medium. This is achieved by iteratively solving the forward problem with improved estimations of the radiative properties until the calculated value converges to the experiment result.<sup>35,36</sup>

#### IV. RESULTS AND DISCUSSION

The deduced extinction coefficient and scattering albedo are shown in Figures 3(A) and 3(B). The inverse problem solving procedure described above was applied to the measured spectra of the eight aerogel samples and the ranges of the deduced properties are plotted as the gray band. The relatively small fluctuations of the deduced properties indicate that they are independent of the sample thickness and can be considered intrinsic properties of the medium. Therefore, only the average value of the deduced extinction coefficient and scattering albedo (solid lines) were used in further analysis.

Based on Eq. (3), the absorption and scattering coefficient were obtained and plotted in Figure 3(C). Clearly, absorption is the dominant extinction mechanism at longer wavelengths while scattering becomes more important in the visible and UV band. The extinction peaks at 1.4  $\mu\text{m}$ , 1.9  $\mu\text{m}$  and 2.2  $\mu\text{m}$  were confirmed to be from absorption by water and silanol groups.<sup>37</sup> Unlike the absorption spectrum which has distinct peaks stemming from discrete vibration modes, the scattering spectrum is a smooth function of wavelength. To study the wavelength dependence, a log-log plot of scattering spectrum is shown in Figure 3(D) with a linear fit from 300 nm to 1000 nm. The scattering coefficient has a  $\lambda^{-4}$  dependence indicated by the slope of the fit. It coincides with the prediction of the Rayleigh-Gans theory, which states that the scattering coefficient can be calculated by<sup>21</sup>

$$\sigma_s = 4\pi^4 \frac{\rho_{\text{ap}}}{\rho_{\text{SiO}_2}} \frac{d^3}{\lambda^4} \left( \frac{n^2 - 1}{n^2 + 2} \right) \quad (6)$$

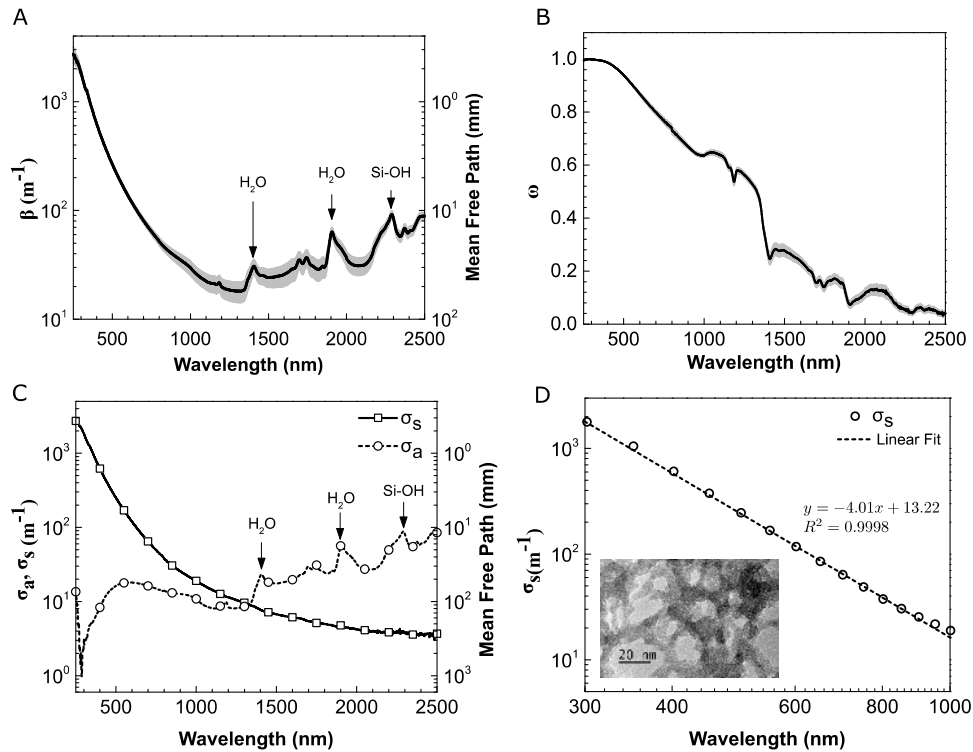


FIG. 3. Deduced (A) extinction coefficient  $\beta$ , (B) scattering albedo  $\omega$  and (C) absorption and scattering coefficient  $\sigma_a$ ,  $\sigma_s$ . Corresponding photon mean free path is shown on the right axis in (A) and (C). The shaded bands in (A) and (B) indicate the range of data calculated based on the measured spectra from samples of different thickness. (D) log-log plot of  $\sigma_s$  as a function of wavelength and a linear fit in the range of 300 nm to 1000 nm. Inset shows a TEM image of the silica nanoparticles from a synthesized aerogel sample (scale bar = 20 nm).

where  $\rho_{ap}$  is the apparent density of the aerogel sample ( $0.084 \text{ g/cm}^3$ ),  $\rho_{\text{SiO}_2}$  is the density of amorphous silica ( $2.2 \text{ g/cm}^3$ ),  $d$  is the diameter of the scattering center,  $\lambda$  is the wavelength, and  $n$  is the relative refractive index of silica to air (1.46).<sup>38</sup>

With all of the known constants in Eq. (6), it is possible to estimate the effective diameter of the scattering center from the intercept  $b$  of the linear fit by the following relation

$$d = 3 \sqrt[3]{\frac{10^{(b-9)}}{4\pi^4 \frac{\rho_{ap}}{\rho_{\text{SiO}_2}} \left(\frac{n^2-1}{n^2+2}\right)}} \quad (7)$$

Note the “-9” is included in the exponent because of unit conversion from nm to m. The effective Rayleigh scattering diameter according to Eq. (7) was found to be 15.9 nm. This effective diameter characterizes the size of Rayleigh scattering centers, which can be directly compared among different samples as an indicator of scattering strength (the smaller the effective size, the weaker the scattering).<sup>20</sup> The TEM image (inset Figure 3(D)) shows that the diameter of silica particles in the sample is around 10 nm. The size discrepancy between the Rayleigh scattering center and real silica particles can be attributed to the fact that in the real material system, particle aggregates form effective scattering centers of larger size.<sup>7,24</sup>

One of the benefits of knowing the intrinsic radiative properties of the aerogel is the capability to predict the transmittance as well as reflectance of a sample with any thickness. The experimentally measured transmittance at 300 nm, as well as the prediction by the B-L law and by the RTE are plotted in Figure 4(A). The B-L law is a straight line in the log scale plot and its slope is determined such that it matches the experiment data for the thinnest aerogel sample. For thicker samples, the B-L law greatly underestimates the transmittance. Although the slope of the B-L law is set arbitrarily, it is clear that in Figure 4(A), the transmittance does not scale linearly with thickness

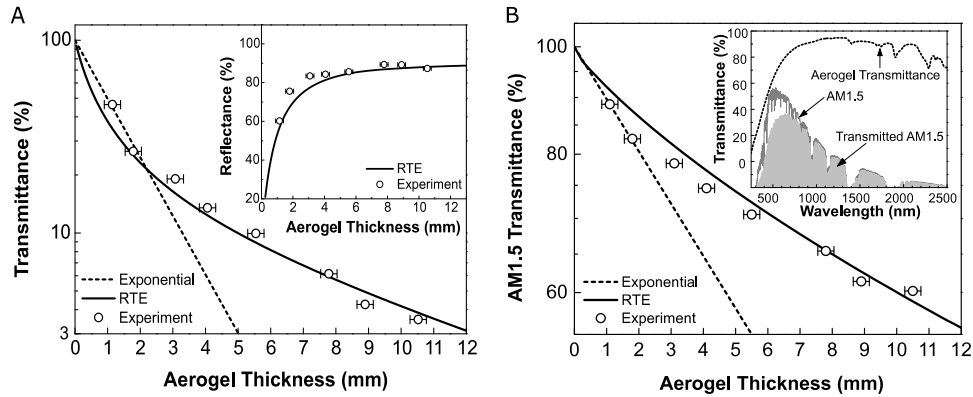


FIG. 4. (A) Hemispherical transmittance at 300 nm as a function of aerogel thickness. Inset also shows the trend for hemispherical reflectance. (B) AM1.5 weighted transmittance as a function of aerogel thickness. Experimentally measured data, prediction by an exponential function as well as RTE are plotted. Inset shows the original, transmitted AM1.5 spectrum as well as the aerogel hemispherical transmittance.

in a log scale plot. In fact, due to strong scattering, the hemispherical transmittance scales in a non-exponential trend with respect to the aerogel thickness. By capturing both the absorption and scattering simultaneously, the RTE model achieves better agreement with experimental data across the entire thickness range. The small differences between the RTE model and experiments can be attributed to two factors. First, the parameters used in the RTE model are the average optical properties of eight samples. Although they were synthesized from the same batch, their properties can vary slightly due to ambient condition fluctuations. Secondly, the scattering contribution from surface inhomogeneity is assumed to be small compared to the bulk contribution.<sup>9</sup> This assumption can break down especially for thin aerogel samples, which can be observed in Figure 4 (where there is a larger discrepancy between model and experiment for thin samples).

In addition to transmittance, by calculating the intensity of backscattered photons, the RTE model can also accurately predict the hemispherical reflectance (inset of Figure 4(A)). The same calculation can be readily extended to other wavelengths by taking the corresponding absorption and scattering coefficient from Figure 3(C) (see supplemental section II).

One useful metric in many solar and glazing technologies is the AM1.5 weighted transmittance, which is defined as

$$\tau_{AM1.5} = \frac{\int AM1.5(\lambda)\tau^h(\lambda)d\lambda}{\int AM1.5(\lambda)d\lambda} \quad (8)$$

The integral in the numerator is the total transmitted AM1.5 spectrum, indicated by the shaded area in the inset of Figure 4(B). Using the predicted hemispherical transmittance spectrum by the RTE model, we can obtain  $\tau_{AM1.5}$  as a function of aerogel thickness (Figure 4(B)). It agrees well with the experimentally determined result. Since absorption peaks due to the presence of water molecules exist in the atmospheric transmission spectra, the water absorption in aerogel do not reduce the overall solar transmission (Figure 4(B) inset). Therefore, scattering in the UV and visible bands becomes the dominant extinction mechanism and thus the B-L law underestimates the AM1.5 transmittance (Figure 4(B)).

Since the obtained radiative properties are intrinsic to the material, they can be used to study photon transport in more general geometries. In this regard, Monte Carlo simulation is a powerful statistical technique to handle complex geometries. As a demonstration, we used the Monte Carlo method and the obtained radiative properties to study the propagation of laser beams in a synthesized aerogel sample of cubic shape. Figure 5 shows the experimentally captured and Monte Carlo simulated<sup>39</sup> photon flux in the aerogel sample (see supplemental section III). Images in the top row are from the experiment where a laser beam was incident on the aerogel sample from the top surface and the side view image was captured by a DSLR camera; images in the bottom row are from 2-D Monte Carlo simulations (where the input radiative properties, shown in the images,

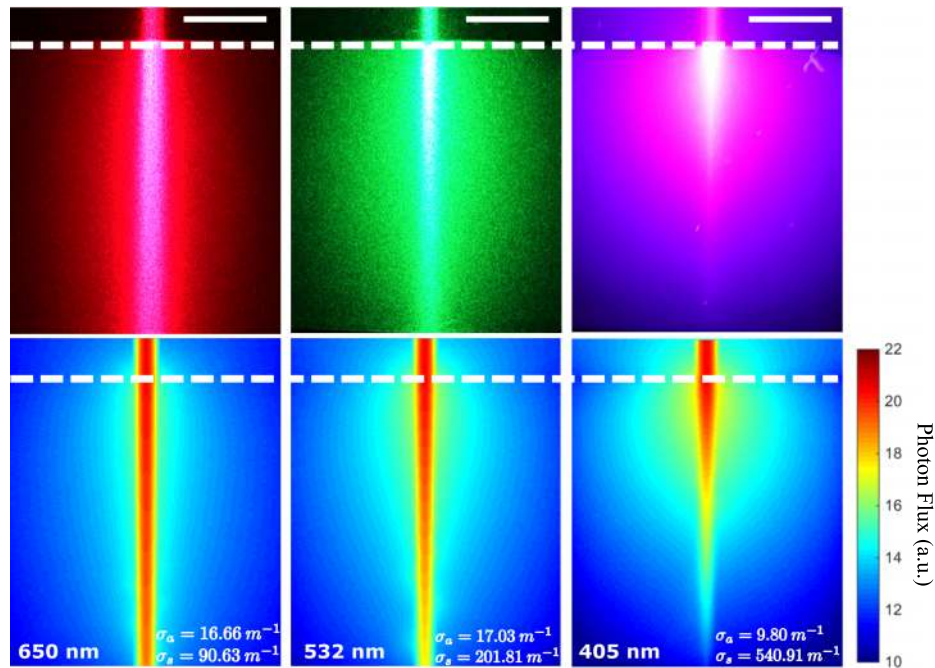


FIG. 5. Top row: side view images of laser beams (650 nm, 532 nm and 405 nm) incident on an aerogel sample (scale bar = 5 mm). Bottom row: Monte Carlo simulated photon flux with the deduced radiative properties as input.

are from Figure 3(C) at corresponding wavelengths). Scattering becomes more significant from the left image to the right as the wavelength decreases. Although this simulation is for a simple cube geometry, the fact that experimental and simulated patterns match validates our conclusion that the radiative properties in Figure 3(C) are intrinsic material properties. Since these properties depend on the microstructure of the silica aerogel and do not change with macroscopic geometry, the same simulation procedure can be applied to aerogels of complex shapes.

## V. SUMMARY

In this study, the radiative properties of silica aerogels were evaluated based on a 1-D RTE model and experimentally measured hemispherical transmittance and reflectance spectra. The obtained properties were found to be independent of the sample geometry and can be considered as the intrinsic material properties. Absorption and scattering were decoupled and quantified separately by calculating the absorption and scattering coefficient. The scattering coefficient showed a  $\lambda^{-4}$  dependence and the effective Rayleigh scatter center diameter was found to be 15.9 nm. Using the obtained radiative properties, we can predict the hemispherical transmittance and reflectance of silica aerogel slabs of any thickness with improved accuracy. Finally, the obtained radiative properties can be used to study the photon transport in silica aerogels of arbitrary geometries by using Monte Carlo modeling.

## ACKNOWLEDGEMENT

We thank Lee Weinstein for useful discussions and Kevin Bagnall for his help on the laser experiment. This work made use of the MRSEC Shared Experimental Facilities at MIT, supported by the National Science Foundation under award number DMR-1419807. This work was supported by the ARPA-E FOCUS program (DE-AR0000471).

<sup>1</sup> C.H. Aerogels, M.A. Aegerter, N. Leventis, and M.A. Koebel, *Aerogels Handbook* (Springer-Verlag, New York, 2011).

<sup>2</sup> A. Soleimani Dorcheh and M.H. Abbasi, *J. Mater. Process. Technol.* **199**, 10 (2008).

<sup>3</sup> J.L. Gurav, I.-K. Jung, H.-H. Park, E.S. Kang, and D.Y. Nadargi, *J. Nanomater.* **2010**, 1 (2010).



- <sup>4</sup> J. Fricke and T. Tillotson, *Thin Solid Films* **297**, 212 (1997).
- <sup>5</sup> A. Nordgaard and W.A. Beckman, *Sol. Energy* **49**, 387 (1992).
- <sup>6</sup> N.D. Kaushika and K. Sumathy, *Renew. Sustain. Energy Rev.* **7**, 317 (2003).
- <sup>7</sup> M. Rubin and C.M. Lampert, *Sol. Energy Mater.* **7**, 393 (1983).
- <sup>8</sup> K. McEnaney, L.A. Weinstein, D. Kraemer, H. Ghasemi, and G. Chen, *Nano Energy* (2015) (submitted).
- <sup>9</sup> G. Pajonk, *J. Non. Cryst. Solids* **225**, 307 (1998).
- <sup>10</sup> G.M. Pajonk, E. Elaloui, B. Chevalier, and R. Begag, *J. Non. Cryst. Solids* **210**, 224 (1997).
- <sup>11</sup> A.J. Hunt, *J. Non. Cryst. Solids* **225**, 303 (1998).
- <sup>12</sup> P. Wang, W. Körner, A. Emmerling, A. Beck, J. Kuhn, and J. Fricke, *J. Non. Cryst. Solids* **145**, 141 (1992).
- <sup>13</sup> E. Aschenauer, N. Bianchi, G. P. Capitani, P. Carter, C. Casalino, E. Cisbani, C. Coluzza, R. De Leo, E. De Sanctis, D. De Schepper, V. Djordjadze, B. Filippone, S. Frullani, F. Garibaldi, J.O. Hansen, B. Hommez, M. Iodice, H.E. Jackson, R. Kaiser, J. Kanetsaka, L. Lagamba, V. Muccifora, E. Nappi, W.D. Nowak, T.G. O'Neill, D. Potterveld, D. Ryckbosch, Y. Sakemi, F. Sato, a. Schwind, K. Suetsugu, T. a. Shibata, E. Thomas, M. Tytgat, G.M. Urciuoli, K. Van De Kerckhove, R. Van De Vyver, S. Yoneyama, and L.F. Zhang, *Nucl. Instruments Methods Phys. Res. Sect. A Accel. Spectrometers, Detect. Assoc. Equip.* **440**, 338 (2000).
- <sup>14</sup> K. Kanamori, M. Aizawa, K. Nakanishi, and T. Hanada, *Adv. Mater.* **19**, 1589 (2007).
- <sup>15</sup> A.R. Buzykaev, A.F. Danilyuk, S.F. Ganzhur, E.A. Kravchenko, and A.P. Onuchin, *Nucl. Instruments Methods Phys. Res. Sect. A Accel. Spectrometers, Detect. Assoc. Equip.* **433**, 396 (1999).
- <sup>16</sup> H. Budunoglu, A. Yildirim, M.O. Guler, and M. Bayindir, *ACS Appl. Mater. Interfaces* **3**, 539 (2011).
- <sup>17</sup> M. Tabata, I. Adachi, Y. Ishii, H. Kawai, T. Sumiyoshi, and H. Yokogawa, *Nucl. Instruments Methods Phys. Res. Sect. A Accel. Spectrometers, Detect. Assoc. Equip.* **623**, 339 (2010).
- <sup>18</sup> T.M. Tillotson and L.W. Hrubesh, *J. Non. Cryst. Solids* **145**, 44 (1992).
- <sup>19</sup> A. Emmerling and J. Fricke, *J. Non. Cryst. Solids* **145**, 113 (1992).
- <sup>20</sup> A. Emmerling, R. Petricevic, A. Beck, P. Wang, H. Scheller, and J. Fricke, *J. Non. Cryst. Solids* **185**, 240 (1995).
- <sup>21</sup> C.F. Bohren and D.R. Huffman, *Absorption and Scattering of Light by Small Particles* (Wiley, 1983).
- <sup>22</sup> H. Yu, D. Liu, Y. Duan, and X. Wang, *Opt. Express* **22**, 7925 (2014).
- <sup>23</sup> G.R. Cunnington and S.C. Lee, *J. Thermophys. Heat Transf.* **12**, 17 (1998).
- <sup>24</sup> S. Lallich, F. Enguehard, and D. Baillis, *J. Heat Transfer* **131**, 082701 (2009).
- <sup>25</sup> See supplementary material at <http://dx.doi.org/10.1063/1.4943215> for detail information on aerogel synthesis, characterization and experiment setup.
- <sup>26</sup> M. Tabata, I. Adachi, H. Kawai, T. Sumiyoshi, and H. Yokogawa, *Nucl. Instruments Methods Phys. Res. Sect. A Accel. Spectrometers, Detect. Assoc. Equip.* **668**, 64 (2012).
- <sup>27</sup> J.S.Q. Zeng, R. Greif, P. Stevens, M. Ayers, and a. Hunt, *J. Mater. Res.* **11**, 687 (1996).
- <sup>28</sup> H.A. Gaonkar, D. Kumar, R. Ramasubramaniam, and A. Roy, *Appl. Opt.* **53**, 2892 (2014).
- <sup>29</sup> T. Fu, J. Tang, K. Chen, and F. Zhang, *J. Heat Transfer* **138**, 032702 (2015).
- <sup>30</sup> H. Yu, D. Liu, Y. Duan, and X. Wang, *Int. J. Heat Mass Transf.* **70**, 478 (2014).
- <sup>31</sup> M. Modest, *Radiative Heat Transfer*, 3rd ed. (Academic, Oxford, 2013).
- <sup>32</sup> B. Davison, *Neutron Transport Theory* (Oxford University Press, London, 1957).
- <sup>33</sup> B.H.J. McKellar and M.A. Box, *J. Atmos. Sci.* **38**, 1063 (1981).
- <sup>34</sup> E. Aschenauer, N. Bianchi, and G. Capitani, *Nucl. Instruments ...* **440**, 338 (2000).
- <sup>35</sup> T.F. Coleman and Y. Li, *SIAM J. Optim.* **6**, 418 (1996).
- <sup>36</sup> S.A. Prahl, M.J.C. van Gemert, and A.J. Welch, *Appl. Opt.* **32**, 559 (1993).
- <sup>37</sup> E. Stolper, *Contrib. to Mineral. Petrol.* **81**, 1 (1982).
- <sup>38</sup> E.D. Palik and G. Ghosh, *Handbook of Optical Constants of Solids* (Academic Press, San Diego, 1998).
- <sup>39</sup> Q. Fang and D.A. Boas, *Opt. Express* **17**, 20178 (2009).